

Investigation of spin rotators in CEPC at Z-pole

Wenhao Xia^{1,2}, Zhe Duan^{1*}, Jie Gao^{1,2*} and Yiwei Wang^{1*}

¹Key Laboratory of Particle Acceleration Physics and Technology, Institute of High Energy Physics, Chinese Academy of Sciences, 19B Yuquan Road, Beijing, 100049, China.

² University of Chinese Academy of Sciences, 19A Yuquan Road, Beijing, 100049, China.

*Corresponding author(s). E-mail(s): duanz@ihep.ac.cn;
gaoj@ihep.ac.cn; wangyw@ihep.ac.cn;

Abstract

Purpose: Longitudinal polarization is an important design aspect of the future 100 km-scale Circular Electron Position Collider (CEPC). Spin rotators are needed in CEPC collider rings to make the beam polarization along the longitudinal direction at the interaction points (IPs). This paper focuses on the design of spin rotators for CEPC at Z-pole (45.6 GeV).

Methods: The design of spin rotators in CEPC at Z-pole is based on solenoid magnets and horizontal bending magnets sections. The coupling of transverse motion introduced by solenoids is compensated with quadrupole lenses. Adjustments have been made to the layout to implement the spin rotators into the collider rings.

Results: Longitudinal polarized beam can be achieved at the IPs with the spin rotators. High degree of polarization is attainable, while the effect of spin rotators on orbital motion is acceptable. The detailed simulation results will be presented.

Conclusion: A solenoid-based spin rotator configuration is designed and integrated into the CEPC collider ring lattice. According to the simulation results, the polarization requirements can be satisfied.

Keywords: Beam Polarization, Spin rotator, electron storage ring, CEPC, Z-pole

2 *Investigation of spin rotators in CEPC at Z-pole*

1 Introduction

As a future lepton circular collider, the Circular Electron Positron Collider (CEPC) is proposed for testing the underlying fundamental physics principles of the Standard Model(SM) and exploring physics beyond the SM [1]. In the Conceptual Design Report (CDR) [2], CEPC is designed as a 100-km double-ring collider with two interaction points (IPs). The operated beam energies are 120 GeV as a Higgs factory, 80 GeV as a W factory and 45.6 GeV for Z-pole.

Particle physics experiments with longitudinally polarized beams in CEPC is an important design aspect for an accurate check of the Standard Model. High longitudinal beam polarization ($>50\%$) is required in the interaction points of CEPC without sacrificing luminosity. In this paper, we focus on the realization of longitudinal polarization at Z-pole. The possibility at even higher energies will be addressed elsewhere.

To realize longitudinally polarized colliding beams, we need to address two major issues, polarized beam generation and proper spin rotations in the collider ring. A highly polarized electron beam ($> 80\%$) can be generated by a polarized electron gun [3], accelerated to full collision energy by the Linac and the Booster. There will be polarization decay during the acceleration in the Booster. A preliminary design of Siberian snakes is under investigation to overcome the depolarization in the Booster [4]. It is an independent research topic and therefore it will be not covered here. Finally the polarized beams are injected into the collider rings. Technically speaking, polarized positron sources are costly or less matured to be applied to CEPC-Z at the moment [4–6]. And in the vast majority of cases, single beam polarization is sufficient, since annihilation occurs when the particles are of opposite helicity, like in the measurement of polarized lepton asymmetries at SLC [7]. An electron with a certain helicity will find a partner for itself. Therefore, it is sufficient to have only one of the colliding beams longitudinally polarized, for example, an electron beam. But there may be technological innovations in the future, which can provide a positron beam with a high degree of polarization and meet the bunch intensity requirements. Then the scheme of electron beam polarization maintenance in the Booster also applies to the polarized positron beam. Hence, we design the longitudinal polarization scheme for both e^- and e^+ beams. In this paper, spin rotators are designed for e^+/e^- beams in the CEPC collider ring at Z-pole, to realize the longitudinal polarized beam at the IPs in the collider rings.

A spin rotator is a device which can rotate the particle spins from vertical to longitudinal or vice versa in storage rings. A pair of rotators around each IP are required to keep the polarization vertical in the arcs and to realize longitudinal polarization at the IP. Spin rotators have been successfully employed at HERA for electron and positron beams [8]. The design of the HERA spin rotators is known as the ‘mini rotator’ [9] which consists of a sequence of alternating vertical and horizontal dipoles. In addition, Spin rotator schemes based on helical dipole magnets have been adopted in RHIC to achieve longitudinal polarization at the interaction points [10]. However, the

beam orbit excursion may be large in those spin rotators with pure transverse magnetic fields. Hence the magnet bore must be large enough to accommodate the excursions. Besides, vertical bending magnetic fields in the spin rotators also introduces vertical dispersion and thus an increase in the vertical emittance. This can lead to a reduction of the equilibrium beam polarization, and might not be compatible with high-luminosity e^+/e^- circular collider designs which favor very flat beams. In addition, a combination of solenoids and horizontal bending magnets can also form a spin rotator, hereafter referred to as “solenoid-based spin rotators”.

A spin rotator including a dedicated horizontal bending magnet section and a dedicated solenoid section, was an alternative design first studied for HERA [11] and later discussed by Ivan Koop [12] for the SuperB project [13]. The asymmetric version of that design has the advantage of minimizing the depolarization effect of strong solenoids. Sergei Nikitin first pointed out such a scheme could be modified and applied in CEPC at Z-pole energy [14, 15], using the fact that the interaction region design features a S-shaped twisted orbit in median plane, so that depolarization of the spin rotators could be largely suppressed. Recently, a solenoid-based spin rotator for the electron-ion collider (EIC) is under study [16]. The scheme consists two spin rotators and two bending arcs on each side of the interaction region. And the design of spin rotators for the electron storage ring allows to realize the exact longitudinal orientation of electron spins in the whole energy range from 5 to 18 GeV [17, 18]. For SuperKEKB, a very compact spin rotator design is under study that consists of solenoid-dipole combined function magnets [19].

In order to avoid those problems introduced by transverse magnetic fields, we will study a solenoid-based spin rotator configuration in this paper. Then its integration into the CEPC collider ring is investigated. In this study, we used a CEPC CDR lattice at Z pole. The SAD code [20] was used in the design of the spin rotator and evaluation of its influence to orbital motion. The Bmad/PTC code [21, 22] was used to evaluate the performance of the spin motion and polarization. It has been verified that lattice translations between SAD and Bmad/PTC provide consistent results by Demin Zhou *et al* [23].

The theories of spin dynamics are reviewed in Section 2. Section 3 presents the designs of solenoid-based spin rotators and two different insertion schemes are compared. In Section 4, the spin rotator design is optimized based on the pros of both insertion schemes, and the simulation results for spin motion and orbital motion are presented. Finally, potential optimization of the spin rotators insertion is analyzed qualitatively.

2 Theory

An beam is polarized if there exists a direction for which the two possible spin states are not equally populated. Polarization is the statistical average of an ensemble of the spin of particles in the beam. Consider a beam consists if N

4 *Investigation of spin rotators in CEPC at Z-pole*

electrons, the polarization degree along a specified axis is given by

$$P = \frac{N_{\uparrow} - N_{\downarrow}}{N} \quad (1)$$

where $N_{\uparrow} - N_{\downarrow} = N$. N_{\uparrow} and N_{\downarrow} are the number of electrons in the up state and down state respectively.

The precession of the spin vector \mathbf{S} of a charged particle with spin- $\frac{1}{2}$ in an electromagnetic field is determined by the Thomas-BMT equation [24, 25]:

$$\frac{d\mathbf{S}}{dt} = \boldsymbol{\Omega} \times \mathbf{S} \quad (2)$$

$$\boldsymbol{\Omega} = -\frac{e}{m_0\gamma} \left[(1 + a\gamma)\mathbf{B}_{\perp} + (1 + a)\mathbf{B}_{\parallel} + (a\gamma + \frac{\gamma}{1 + \gamma}) \frac{\mathbf{E} \times \mathbf{v}}{c^2} \right]$$

where $\mathbf{B} = \mathbf{B}_{\parallel} + \mathbf{B}_{\perp}$, $\mathbf{B}_{\parallel} = (\mathbf{v} \cdot \mathbf{B})\mathbf{v}/v^2$. m_0 and e is the mass and charge of the particle. a is the anomalous magnetic moment, $a = 0.00115965$ for electron and positron. γ is the relativistic factor. c is the speed of light.

When t is replaced by the azimuthal angle θ , one special solution of Eq.(2) is the invariant spin field [26], $\mathbf{n}(\mathbf{u}; \theta)$, satisfying the periodic condition $\mathbf{n}(\mathbf{u}; \theta + 2\pi) = \mathbf{n}(\mathbf{u}; \theta)$, \mathbf{u} is the phase space coordinate in terms of canonical variables of the orbital motion. The rate of spin precession around \mathbf{n} is described by the amplitude dependent spin tune ν_s [26]. On the closed orbit, $\mathbf{n}(\mathbf{u}; \theta)$ and ν_s reduces to $\mathbf{n}_0(\theta)$ and ν_0 , respectively. In a planar storage ring, $\mathbf{n}_0(\theta)$ is close to the vertical direction, and $\nu_0 \approx a\gamma$.

The spin motion may be perturbed in a resonant manner when the following condition is satisfied,

$$\nu_s = k + k_x\nu_x + k_y\nu_y + k_z\nu_z, \quad k, k_x, k_y, k_z \in \mathbb{Z} \quad (3)$$

where ν_x, ν_y, ν_z are the horizontal, vertical betatron tunes and synchrotron tune, respectively. Spin resonances with $\nu_s = k, k \in \mathbb{Z}$ are called integer spin resonances. Spin resonances with $|k_x| + |k_y| + |k_z| = 1$ and $|k_x| + |k_y| + |k_z| > 1$ are called first-order spin resonances and higher-order spin resonances, respectively. In particular, synchrotron sideband spin resonances $\nu_0 \pm \nu_u + m\nu_z = k$, with $|m| > 1$ and $u = x, y$ are considered very important in high-energy electron storage rings [27].

In an electron storage ring, a spontaneous buildup of radiative polarization may occur via the emission of spin-flip synchrotron radiation. This process is called the Sokolov-Ternov effect [28]. However, the stochastic photon emission also leads to the spin diffusion effect [29]. The equilibrium polarization [30] is a balance between the Sokolov-Ternov effect and the spin diffusion effect, its direction is along $\langle \mathbf{n} \rangle_{\theta}$, which is an average over phase space at the azimuthal angle θ . Generally speaking, $\langle \mathbf{n} \rangle_{\theta}$ is very nearly aligned along $\mathbf{n}_0(\theta)$. The degree

of the equilibrium polarization can be approximated by

$$P_{\text{eq}} \approx \frac{P_{\infty}}{1 + \frac{\tau_p}{\tau_d}} \quad (4)$$

where P_{∞} equals to 92.4% in an ideal planar ring. And the equivalent polarization build-up time is

$$\frac{1}{\tau_{\text{tot}}} = \frac{1}{\tau_p} + \frac{1}{\tau_d} \quad (5)$$

τ_p and τ_d are the time constants for the Sokolov-Ternov effect and spin diffusion effect, respectively. For the CEPC collider ring at Z-pole. $\tau_p \approx 260$ hours. According to Eq.(4) and (5), if the equilibrium polarization equals to 50%, we can get $\tau_d \approx 310$ hours and the equivalent polarization build-up time $\tau_{\text{tot}} \approx 141$ hours.

For the CEPC collider rings, top-up injection mode will be used to maximize the integrated luminosity [2]. Time-averaged beam polarization in an electron storage ring during the top-up injection is [31]

$$P_{\text{avg}} = \frac{P_{\text{eq}}}{1 + \tau_{\text{tot}}/\tau_b} + \frac{P_{\text{inj}}}{1 + \tau_b/\tau_{\text{tot}}} \quad (6)$$

Here P_{inj} is the injected beam polarization, τ_b is the beam lifetime. For colliding beams at Z-pole, the beam lifetime is about 2 hours, mainly limited by the radiative Bhabha effect which is correlated to the luminosity. Hence, if the equilibrium polarization is larger than 10%, τ_{tot} is longer than 28 hours, still significantly longer than the beam lifetime. In this case, if the polarization of the injected beam is very high (for example, more than 70%), then the time-averaged beam polarization is approximately the injected beam polarization. In other words, to maintain a high time-averaged beam polarization, it is essential to realize a high injected beam polarization, while it is only required to achieve a modest equilibrium beam polarization in the collider ring.

3 Solenoid-based spin rotators

According to Eq. (2), the rotation angle of an electron spin vector in a solenoid can be described by

$$\varphi_{\text{sol}} = \frac{e(1+a)}{m_0 c \beta \gamma} \int B_{\parallel} ds \quad (7)$$

And the axis of rotation is along the longitudinal direction. In a horizontal bending dipole, the spin rotation angle is

$$\varphi_{\text{dip}} = \frac{ea}{m_0 c \beta} \int B_y ds = a \gamma \theta \quad (8)$$

6 *Investigation of spin rotators in CEPC at Z-pole*

where θ is the deflection angle of orbital motion. And the axis of rotation is along the vertical direction.

We use one typical design of solenoid-based spin rotators that consists of a solenoid section and a horizontal bending dipole magnet section. In the spin rotator upstream of the IP (RotatorU), the solenoid section rotates the spin vector from the vertical direction to the radial direction with a rotation angle of $\pi/2$. Then the horizontal bending magnet section rotates the spin vector by an odd multiple of $\frac{\pi}{2}$, i.e.

$$\varphi = (2K + 1)\frac{\pi}{2}, \quad K \in \mathbb{Z} \quad (9)$$

which can rotates the spin vector from the radial direction to the longitudinal direction at the IP. Rotation of a spin vector from the longitudinal direction at the IP, to the vertical direction in the arc can be realized by a spin rotator downstream of the IP (RotatorD), with a similar setup of RotatorU, but in a reversed order. Such a pair of spin rotators can realize longitudinal beam polarization at IPs, while retaining vertical beam polarization in the arc regions.

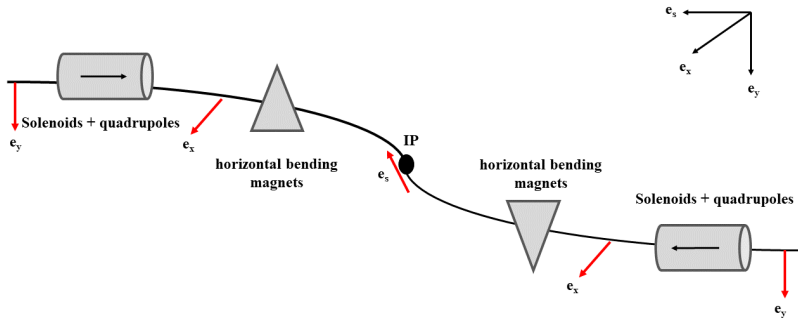
There are two possibilities of arrangement of a pair of spin rotators around each IP [11], in terms of whether the spin rotators on both sides of the IP are mirror-symmetric, as illustrated in Fig. 1. Compared with the symmetric arrangement, the asymmetric arrangement can exactly rotate the spin vector back to the vertical direction in the arc even when not running at the designed energy. In addition, the asymmetric structure also matches the geometry of the CEPC collider ring in the interaction region (IR). Therefore, the asymmetric arrangement is preferred when the spin rotators are placed near the interaction region. The symmetric arrangement is also investigated for CEPC, and it will be discussed below.

To rotate the spin vector by $\pi/2$ at $E = 45.6$ GeV, the required integrated field strength of the solenoid magnets is about $240 \text{ T} \cdot \text{m}$. For example, if we consider a solenoid magnetic field of 8 T using superconducting technology, the total length of the solenoid magnet is about 30 m. This requires a series of solenoid magnets.

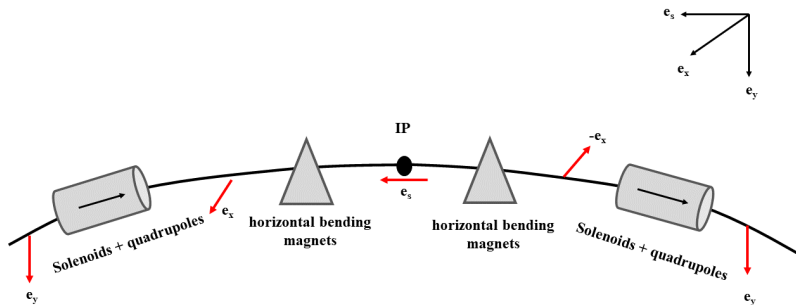
3.1 Designs of the solenoid section

Solenoids introduce transverse coupling which is detrimental to both the orbital and spin motion, which must be compensated locally. There are different possibilities to compensation schemes using quadrupoles lens [32]. We designed two possible solenoid compensation units (SCUs), as shown in Fig. 2. Accordingly, a solenoid module is design to include a series of SCUs to rotate the spin vector by $\frac{\pi}{2}$ in the middle, as well as optics matching sections (OM) at both ends, to match with the optical parameters of the CEPC collider ring lattice.

Solenoid compensation unit 1 (SCU1) consists of two solenoids with 7 normal quadrupoles in between. With the magnet parameters listed in Fig. 2(a),



(a) Asymmetric arrangement.



(b) Symmetric arrangement.

Fig. 1 Two possible arrangements of the spin rotator magnets. The red arrow represents the direction of polarization. Here e_x , e_s , and e_y are the radial, longitudinal, and vertical unit base vectors, respectively.

SCU1 can rotate the spin vector by $\varphi = \frac{\pi}{20}$. According to the 4×4 transport matrices shown in Fig. 2, SCU1's effect on orbital motion is equivalent to that of a drift of equal length with an extra phase advance of π in the vertical direction. Solenoid module 1 (SM1) is designed to contain 10 SCU1s to rotate the spin vector by $\pi/2$, its whole structure is

$$\text{OM} + 5 \times (\text{QD} + \text{SCU1} + \text{QF} + \text{QF} + \text{SCU1} + \text{QD}) + \text{OM}$$

Here “QD” and “QF” mean defocusing and focusing quadrupoles, respectively. Each OM contains six normal quadrupoles to fit into the optics of the ring

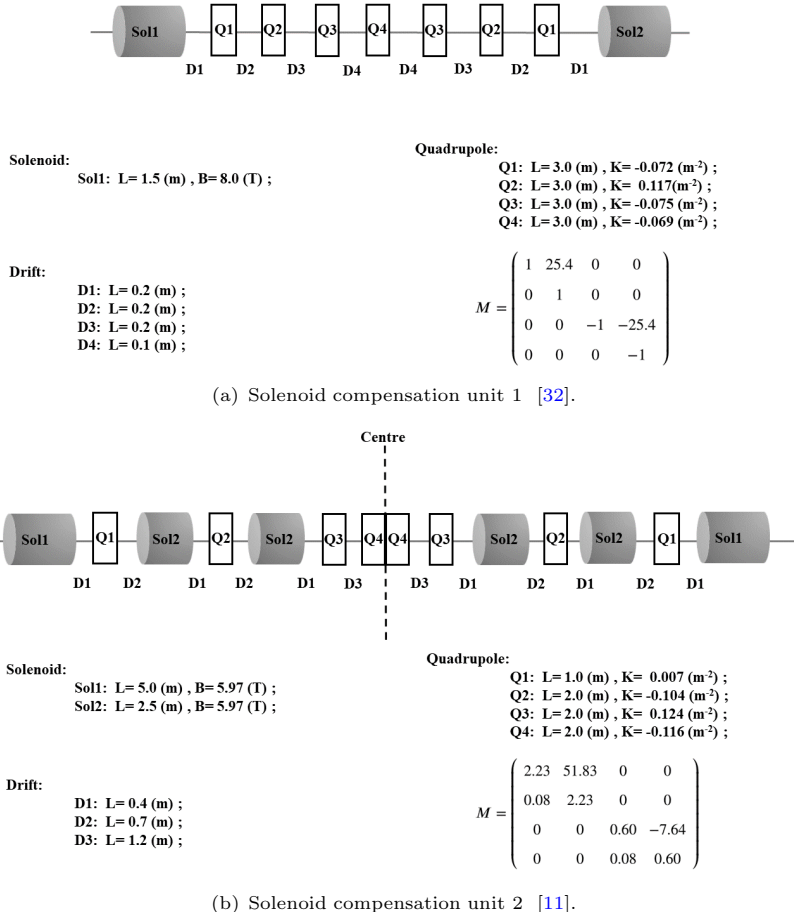
8 *Investigation of spin rotators in CEPC at Z-pole*

Fig. 2 Two solenoid compensation units. Magnet parameters are listed in each subfigure. M is the transverse transport matrix for each unit.

lattice. The quadrupoles and solenoids in SCU1s can be just turned off for operation without longitudinal polarization or for other operated energies.

Solenoid compensation unit 2 (SCU2) consists of 6 solenoids interleaved with 8 normal quadrupoles, with a spin rotation angle of $\varphi = \frac{\pi}{4}$. Solenoid module 2 (SM2) is designed to contain 2 SCU2s to rotate the spin vector by $\pi/2$, its whole structure is

$$\text{OM} + \text{SCU2} + \text{D} + \text{QF} + \text{D} + \text{QF} + \text{D} + \text{SCU2} + \text{OM}$$

“D” is an abbreviation for drift. Each OM contains three normal quadrupoles to fit into the optics of the ring lattice. If the solenoids are turned off, the

quadrupoles in SCU2s need be retuned to create a normal uncoupled optics with designed phase advances.

OM and the quadrupoles are adjusted to match the optics at the entrance and exit of solenoid modules. lattice structures and the twiss parameters in the two solenoid modules are plotted in Fig. 3. Table 1 compares the key

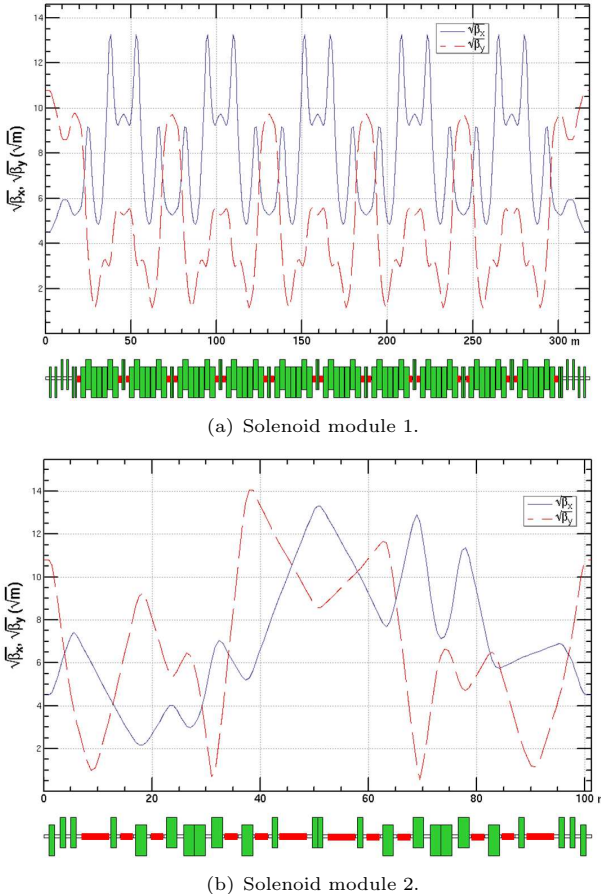


Fig. 3 Twiss parameters and lattice structures for two solenoid modules. Green and red boxes represent normal quadrupoles and solenoid magnets respectively.

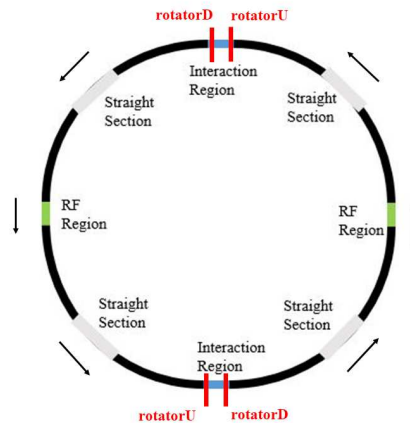
parameters of SM1 and SM2. SM2 is 220 meters shorter than SM1, and uses much less magnets.

3.2 Insertion schemes

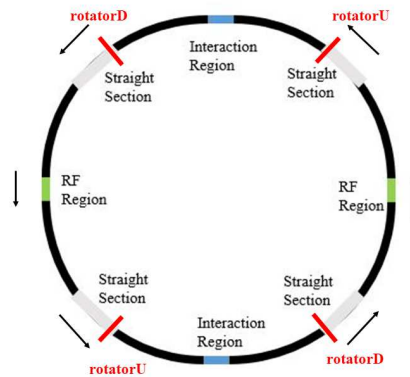
According to Eq.(9), the spin rotation around the vertical axis from IP to the solenoid module is $(2K + 1)\frac{\pi}{2}$. This requires adjustments to the layout of the collider ring between the solenoid module insertions. Two possible insertion

Table 1 The structure comparison of the solenoid module 1 and module 2.

	Solenoid module 1	Solenoid module 2
Number of quadrupoles per unit	7	8
Number of solenoids per unit	2	6
Number of solenoid compensation units	10	2
Total length (m)	320	100



(a) Insertion scheme 1: spin rotators inside the IR [33].



(b) Insertion scheme 2: spin rotators in the straight section next to IR.

Fig. 4 Two insertion schemes for spin rotators. Black arrows represent the direction of beam movement. Red lines are spin rotators, while “rotatorU” and “rotatorD” represent the spin rotators upstream and downstream of the IP, respectively. The black curve represents the arc area.

schemes of SM1 are studied and compared in this section. Fig. 4 shows the

positions of spin rotators in one ring of CEPC. The solenoid section are placed inside the IR in Fig. 4(a), forming an anti-symmetric arrangement. In contrast, the solenoid section are placed in the straight sections adjacent to the IR in Fig. 4(b), forming an anti-symmetric arrangement. We'll describe in more detail about these two configurations. The layout of one interaction region (IR) of the CEPC lattice is shown in Fig. 5. The default parameters in Fig. 5 are

- $\theta_c = 16.50$ mrad, half of the crossing angle between e^+ ring and e^- ring at the IP;
- $\theta_u = -19.21$ mrad, the total horizontal bending angle from the IP to the end of the interaction region “MIRU”;
- $\theta_d = 29.35$ mrad, the total horizontal bending angle from the IP to the sextupole “SC0IRD”;
- $\theta_{dd} = -15.56$ mrad, the total horizontal bending angle from the sextupole “SC0IRD” to the end of the interaction region “MIRD”;
- $\theta_{\text{IR}} = -2.71$ mrad, the angle between the end direction of the IR and the horizontal coordinates of global geometry.

First, we consider to implement the solenoid section inside the interaction regions. In particular, there are straight sections after “SC0IRD” and “SC0IRU” which can be modified to insert SM1. This however requires modification of the bending angle θ_u and θ_d . We multiple the bending angles of all the bending magnets that contribute to θ_u and θ_d by C_1 and C_2 , respectively. To make \mathbf{n}_0 along the longitudinal direction at the IP, the following adjustments must be satisfied

$$\begin{aligned} a\gamma C_1 \times \theta_u &= (2K_1 + 1)\frac{\pi}{2} \\ a\gamma C_2 \times \theta_d &= (2K_2 + 1)\frac{\pi}{2} \end{aligned} \quad (10)$$

where $K_1, K_2 \in \mathbb{Z}$.

The electron ring and the positron ring must not cross each other and must be parallel outside the interaction region with a radial separation $D = 0.35$ m.

$$\begin{aligned} \theta_{\text{IR}} &= -\theta_c + C_2\theta_d + \theta_{dd} = \theta_c + C_1\theta_u \\ GX_{\text{MIRD}} &= GX_{\text{MIRU}} + D \times \sin \theta_{\text{IR}} \\ GY_{\text{MIRD}} &= GY_{\text{MIRU}} - D \times \cos \theta_{\text{IR}} \end{aligned} \quad (11)$$

Here “GX” and “GY” the global geometry coordinates in the horizontal plane.

Eq. (10) shows that the values of K_1 and K_2 affect the adjustment. Note that $\theta_u < 0$, hence the value of K_1 must be negative to avoid synchrotron radiation from the upstream bending magnets hitting the IP [34]. And K_2 must not be negative. C_1 , C_2 , and θ_{IR} can be calculated for different values of K_1 and K_2 . We plot geometries of the e^+/e^- rings on one side of the interaction region for different K_1 and K_2 in Fig. 6. The electron ring and positron ring do not cross each other only when $K_1 = -1$, $K_2 = 0$. Then we

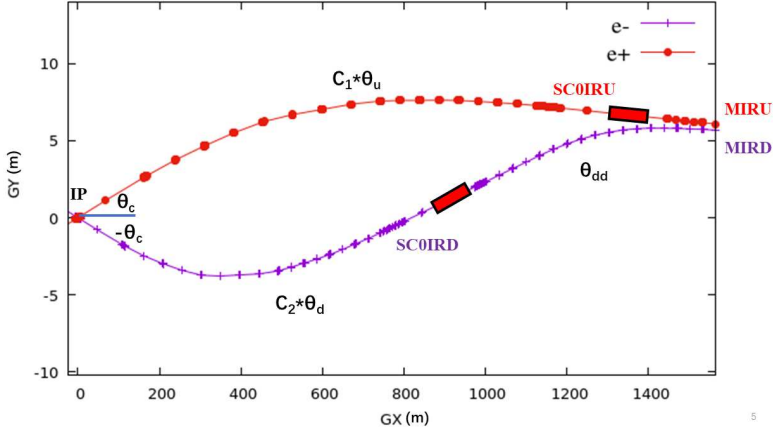


Fig. 5 Geometry of the e^+/e^- rings on one side of the interaction region. The red rectangle represents the spin rotators. These two insertion sites have straight regions long enough to accommodate the spin rotators.

got $C_1 = 0.79$, $C_2 = 0.52$, which are significantly different from 1, so that the change is nontrivial. This will be referred to as insertion scheme 1 hereafter.

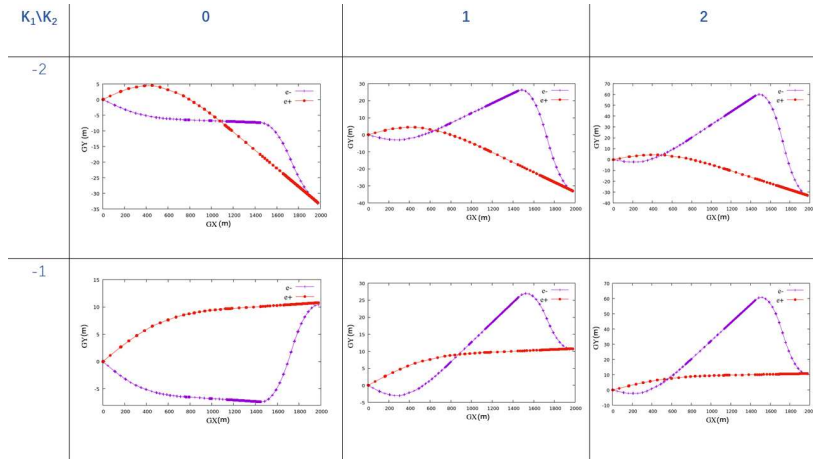


Fig. 6 Geometry of the e^+/e^- rings on one side of the interaction region for different K_1 and K_2 .

Alternatively, we consider to implement the solenoid section in the straight sections next to the IR, as shown in Fig. 4(b). In one arc the orbital deflection angle is $\theta_{ARC} = 786.75$ mrad, corresponding to a spin rotation angle of approximately $2 \times 26 * \frac{\pi}{2}$. In order to change the CEPC lattice as little as

possible, the following formulas need to be satisfied

$$\begin{aligned} a\gamma(C_u\theta_u + \theta_{\text{ARC}} + 2\theta_b) &= (2 \times 25 + 1)\frac{\pi}{2} \\ a\gamma(\theta_d + C_{dd}\theta_{dd} + \theta_{\text{ARC}} + 2\theta_b) &= (2 \times 26 + 1)\frac{\pi}{2} \end{aligned} \quad (12)$$

Here we inserted an extra regular arc FODO cell with a horizontal bending angle $2\theta_b$ just before the dispersion suppressor adjacent to the straight section where the solenoid section is implemented. And $\theta_b = 2.68$ mrad. We multiple the bending angles of all the bending magnets that contribute to θ_u and θ_{dd} by C_u and C_{dd} , respectively.

Besides, the parallel condition for the e^+ ring and the e^- ring can be described by

$$\begin{aligned} \theta'_{\text{IR}} &= -\theta'_c + \theta_d + C_{dd}\theta_{dd} = \theta'_c + C_u\theta_u \\ GX_{\text{MIRD}} &= GX_{\text{MIRU}} + D \times \sin \theta'_{\text{IR}} \\ GY_{\text{MIRD}} &= GY_{\text{MIRU}} - D \times \cos \theta'_{\text{IR}} \end{aligned} \quad (13)$$

Then we can get $C_{dd} = 1.10$, $C_u = 0.94$, only a modest modification to the bending magnets are needed. However, the crossing angle at IP also need to be adjusted,

$$2\theta'_c = (2 \times 26 - 2 \times 25)\frac{\pi}{2} \frac{1}{a\gamma} \quad (14)$$

$\theta'_c = 15.18$ mrad when $a\gamma = 103.5$. Hereafter this design will be referred to as insertion scheme 2.

After inserting the spin rotators into the collider ring lattice, we also retuned several quadrupoles to recover the fractional part of the betatron tune, $\nu_x = 0.11$, $\nu_y = 0.22$, though an increase in the integer parts of the betatron tunes is inevitable. Table 2 compares the key orbital parameters between insertion scheme 1, insertion scheme 2 and the CDR lattice. The horizontal emittance is increased by an order of magnitude in insertion scheme 1, which can seriously affect the luminosity. In comparison, the influence of insertion scheme 2 on orbital parameters are quite small.

Table 2 The comparison of several key orbital parameters between insertion scheme 1, insertion scheme 2 and the CDR lattice.

	CDR Lattice	Insertion scheme 1	Insertion scheme 2
Tunes $\nu_x/\nu_y/\nu_z$	363.11/365.22/0.028	377.11/379.22/0.0313	379.11/381.22/0.02799
Emittances ϵ_x/ϵ_z	0.18 nm/0.886 μm	1.37 nm/1.089 μm	0.17 nm/0.883 μm
Momentum compact factor α_c	1.11×10^{-5}	1.22×10^{-5}	1.089×10^{-5}
Circumference (m)	100016.35	101290.15	101563.73
SR energy loss per turn U_0 (MeV)	35.74	40.12	35.95
β -function at IPs β_x^*/β_y^*	0.2/0.001	0.2/0.001	0.2/0.001

Then, the performance of spin motion are also evaluated. The projection of \mathbf{n}_0 at the IPs and the equilibrium polarization are simulated by Bmad for both

insertion schemes. Note that the SLIM algorithm implemented in Bmad only considers the spin resonances up to the first order in the equilibrium polarization calculations. As shown in Fig. 7 (a) and (c), the two IPs are located at $s = 0$ and $s = 50$ km, respectively. Both insertion schemes enable longitudinal polarization at the IPs. For insertion scheme 2, the polarization direction has been rotated many turns by the horizontal bending magnets between the IP and the solenoid section, which enhances the spin diffusion effect. Hence the equilibrium polarization degree for insertion scheme 2 is much lower than that of insertion scheme 1. Therefore, the spin rotators must be placed as close as possible to the IP to maintain a high equilibrium beam polarization.

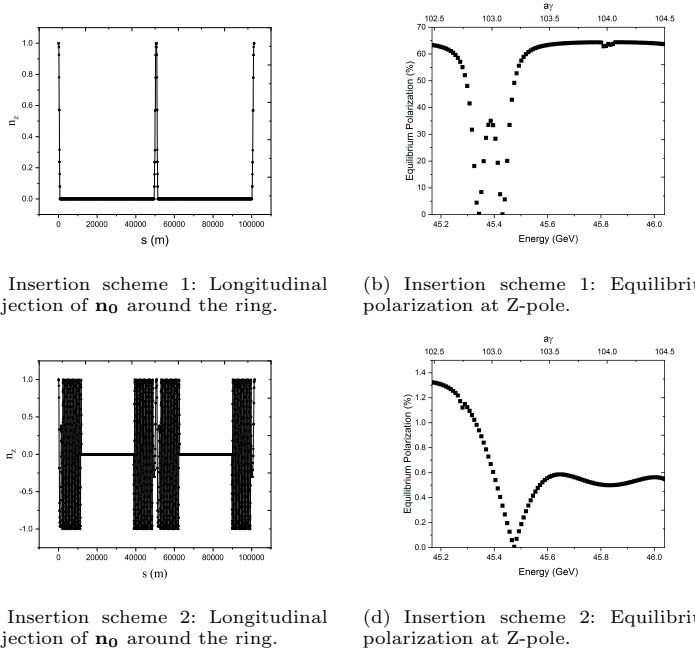


Fig. 7 Longitudinal project of \mathbf{n}_0 around the ring and equilibrium polarization at Z-pole by Bmad. (a) and (b) are the results for insertion scheme 1, while (c) and (d) are the results for insertion scheme 2.

4 Optimization of insertion scheme

In this section, we will optimize the design based on the pros of both insertion schemes. In particular, the solenoid section is placed adjacent to IR. This on one hand eliminates the perturbation to the IR optics, on the other hand reduces the depolarization contribution between the IP and the solenoid section. This optimization scheme can achieve high level of beam polarization

at the IP without affecting the stability of the beam orbital motion. In addition, the solenoid module 2 is utilized here to shorten the length of the spin rotator.

The layout and the optics of IR will remain unchanged. Just upstream of the IR, we insert a bending angle compensation section $\Delta\theta_1$, a straight section (SS) of the same length as the solenoid module, a bending angle compensation section $\Delta\theta_2$ and the solenoid module (rotatorU) in sequence. Just downstream of the IR, we insert a bending angle compensation section $\Delta\theta_1$, the solenoid module (rotatorD), a bending angle compensation section $\Delta\theta_2$ and a SS in sequence. More details of the optimized insertion scheme are plotted in Fig. 8.

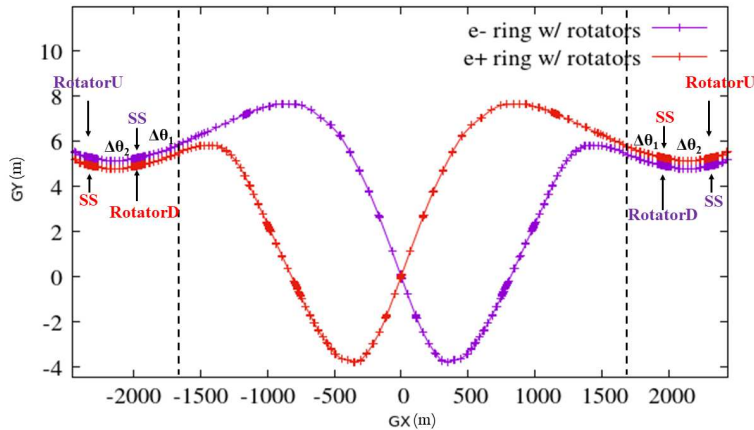


Fig. 8 Geometry of the e^+/e^- rings with spin rotators of the optimized insertion scheme around the IR.

The lattice structure of SS is basically the same as that of the solenoid module. However, the solenoid magnets are replaced with drifts of same length. And the quadrupoles inside the SS are retuned to create a normal uncoupled optics which is matched to the collider ring.

The angle compensation sections $\Delta\theta_1$ and $\Delta\theta_2$ are designed as achromat modules. Each section consists of 4 identical FODO cells with $\frac{\pi}{2}$ phase advances for both planes, to ensure that the dispersion function inside the solenoid module is zero. The dipoles in these FODO cells are as long as the dipoles in the arc FODO cells. However, the magnetic field strength is about an order of magnitude weaker than the arc dipoles.

Now the parallel condition of the positron ring and the electron ring outside the IR is satisfied. And the longitudinal polarization condition requires

$$\begin{aligned} a\gamma(\theta_u + \Delta\theta_1 + \Delta\theta_2) &= -\frac{\pi}{2} \\ a\gamma(\theta_d + \theta_{dd} + \Delta\theta_1) &= \frac{\pi}{2}. \end{aligned} \quad (15)$$

We can get $\Delta\theta_1 = 1.39$ mrad, $\Delta\theta_2 = 2.65$ mrad when $a\gamma = 103.5$.

We then retuned several quadrupoles to recover the fractional part of the betatron tunes of the lattice. And the deflection angles of the dipoles in the rest part of the collider ring are reduced accordingly to ensure the total horizontal deflection angle of the entire ring is 2π . Next, we evaluate the performance of this lattice design via detailed simulations.

4.1 Polarization simulation by Bmad/PTC

Spin rotators can drive betatron sideband spin resonances and lead to a lower equilibrium polarization in the nearby region even for a perfect storage ring. The electrons and positrons execute betatron oscillations, and they are subjected to additional magnet fields as they go through quadrupoles and solenoids. And their spin precession acquires a small additional orbit-dependent component. In particular, between the solenoid sections around each IP, \mathbf{n}_0 is in the horizontal plane, the horizontal betatron oscillations in quadrupole magnets, lead to spin precession around the vertical direction, perpendicular to \mathbf{n}_0 . Hence, this drives first-order betatron sideband spin resonances $\nu_0 = k \pm \nu_x$.

In a real storage ring, the solenoid magnetic field may be not perfectly compensated due to magnets' errors. These magnet errors also drive spin resonances and lead to a reduced equilibrium beam polarization. Assuming that these magnet errors follow a Gaussian distribution in the solenoid compensation unit 2, we introduced relative field errors for solenoids and quadrupoles with a root-mean-squared value of 0.05%, and relative roll errors for quadrupoles with a root-mean-squared value of 0.01%.

We compared the longitudinal projection of beam polarization at the IP and the equilibrium polarization at Z-pole in Fig. 9. As shown in Fig. 9(a), The longitudinal projection of \mathbf{n}_0 at the IP is symmetrically distributed on both sides of the designed energy, $a\gamma = 103.5$. The influence of the magnet errors is negligible. Fig. 9(b) shows the comparison between the equilibrium beam polarization simulated with SLIM inside Bmad, for the cases without magnet errors and with magnet errors. The equilibrium polarization degree can be very high when the beam energy is far from spin resonances. The magnet errors enhance the depolarization near spin resonances. However, they have no effect on the degree of polarization when the fractional part of $a\gamma$ is near 0.5. This shows the robustness of the design against machine imperfections. Besides, Fig. 9(c) shows the influence of higher-order spin resonances on equilibrium beam polarization, relative to the simulation results with SLIM. Here, depolarization effects of the higher-order spin resonances are simulated by a Monte-Carlo method based on PTC [35]. The spin resonance regions where the equilibrium polarization level is low becomes wider and higher-order synchrotron sideband spin resonances are visible.

Other kinds of machine imperfections also affect the orbital motion and the degree of equilibrium polarization, a systematic approach of error correction is under development [36]. Evaluation of the influence of these errors on the

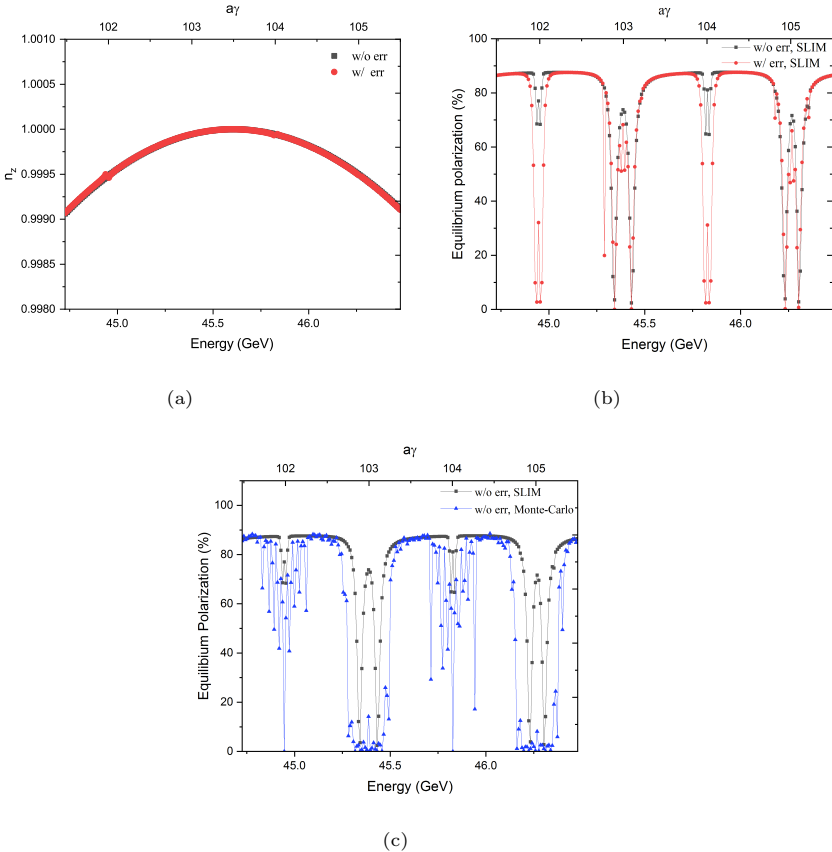


Fig. 9 Polarization simulation results for the optimized insertion scheme. (a) shows the longitudinal projection of \mathbf{n}_0 at the IP for different beam energies, for the lattices with and without magnet errors. (b) compares the equilibrium beam polarization at different beam energies, for the lattices with and without magnet errors, simulated using SLIM in Bmad. (c) compares the equilibrium beam polarization for the lattice without magnet errors, simulated using SLIM in Bmad and Monte-Carlo method in PTC, respectively. The step size $\Delta a\gamma = 0.02$.

equilibrium polarization for a CEPC lattice without spin rotators is reported in [37], which shows a relatively high beam polarization is achievable at Z-pole energy after the error correction. In future studies, we will introduce machine imperfections for the whole collider ring with spin rotators and evaluate the performance after a dedicated correction scheme.

The time-averaged beam polarization is determined by the equilibrium polarization and the injected beam polarization according to Eq.(6), which can also be expressed as

$$P_{\text{avg}} = \frac{P_{\text{eq}}}{1 + \frac{P_{\text{eq}} \tau_p}{P_{\infty} \tau_b}} + \frac{P_{\text{inj}}}{1 + \frac{P_{\infty} \tau_b}{P_{\text{eq}} \tau_p}}. \quad (16)$$

For CEPC at Z-pole, $\tau_p \approx 260$ hours and $\tau_b \approx 2$ hours. If the injected beam polarization degree is 70%, the equilibrium polarization only needs to be greater than 1.8% to maintain the time-averaged polarization larger than 50%. There is quite a large margin from the current simulation results of the equilibrium beam polarization, which reserves tolerance for other potential depolarization mechanisms, for example the influence from beam-beam interaction [38], which will be evaluated separately. The above simulations indeed confirm the analysis that depolarization effects could be largely suppressed in such an anti-symmetric structure in Ref. [14, 15].

4.2 Influence to orbital motion

The optics of the spin rotator insertion and the collider ring is shown in Fig. 10. The betatron motion is only locally coupled in the spin rotators, while the optics of the rest of the collider ring remains undisturbed.

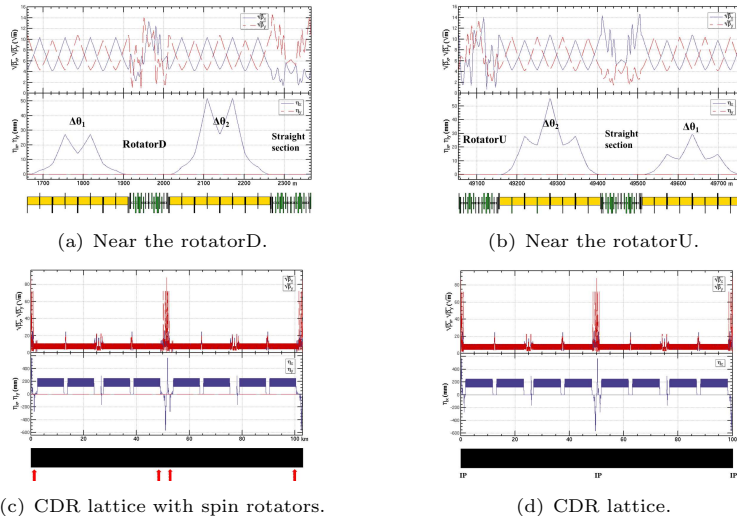


Fig. 10 The optics of the rotator insertion and the collider ring with spin rotators. The red arrows mark the position of spin rotators.

To evaluate the influence of the spin rotators on the orbital motion performance. We consider three different cases. The first is the CEPC CDR lattice without spin rotators (denoted as CDR lattice), the second is the CEPC CDR lattice with spin rotator insertions to realize longitudinal beam polarization (denoted as Solenoid On), the third is the CEPC CDR lattice with spin rotator insertions, but the solenoids are turned off and quadrupoles are retuned to recover the lattice (denoted as Solenoid Off).

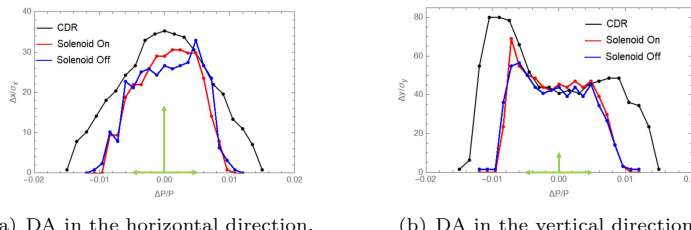
Table 3 compares the key orbital parameters between these three cases. There is an increase in the integer parts of the betatron tunes of the latter two cases, and some tiny differences in the momentum compact factor and U_0 .

The circumference of the collider ring increases by approximately 2.8 kilometers in the presence of the spin rotators. There is no difference in the orbital parameters between Solenoid off and Solenoid on.

Table 3 The comparison of several key orbital parameters between the optimized insertion scheme and the CDR lattice at Z-pole .

	CDR Lattice	Solenoids On	Solenoids Off
$Tunes \nu_x/\nu_y/\nu_z$	363.11/365.22/0.028	381.11/383.22/0.028	381.11/383.22/0.028
Emittances ϵ_x/ϵ_z	0.18 nm/0.886 μ m	0.18 nm/0.886 μ m	0.18 nm/0.886 μ m
Momentum compact α_p	1.11×10^{-5}	1.07×10^{-5}	1.07×10^{-5}
Circumference (m)	100016.35	102841.95	102841.95
SR energy loss per turn U_0 (MeV)	35.47	35.91	35.91
β -function at IPs β_x^*/β_y^*	0.2/0.001	0.2/0.001	0.2/0.001

Furthermore, we examine the effect of the spin rotator on the nonlinear performance of the lattice. The leading orders of the chromaticity have been corrected by adjusting the sextupoles in the arc sections with SAD. We tracked the particles for one damping time (about 2600 turns) to obtain the dynamic apertures, are shown in Fig. 11. Spin rotators in the collider ring leads to a moderate shrink of the dynamic apertures. Since the requirement on dynamic aperture at Z-pole is $17\sigma_x \times 9\sigma_y \times 0.49\%$ according to the CEPC CDR, the shrink is still acceptable. The change in the dynamic aperture for Solenoid Off is tiny compared to that for Solenoid On. This means that the effect of the solenoid magnets on the nonlinear performance of the lattice is compensated by the quadrupoles in the solenoid compensation unit. The dynamic aperture can be further optimized using more families of sextupoles, which is a conventional step in the lattice optimization.



(a) DA in the horizontal direction.

(b) DA in the vertical direction.

Fig. 11 Comparison of the dynamic apertures between the CDR lattice and the CDR lattice with spin rotators (solenoid on/off). The green arrows represent the requirement on dynamic apertures at Z-pole.

5 Potential optimization of the spin rotators insertion

In the above study, we present a complete spin rotator design design and insertion scheme. However the insertion scheme still has the potential for further optimization, especially in terms of the total length.

As we described earlier, the dipole length in the bending angle compensation sections is the same as the arc dipole, while the magnetic field is an order of magnitude weaker. Hence, we can reduce the length of the bending angle compensation sections. For example, if we reduce the length of this sections by a factor of five, from 250 meters to 50 meters. Then the beta functions at the beginning and end of the sections will also be reduced by five times. We can insert triplet cells at both ends of the section to match the optical parameters to the rest of the collider ring. According to a simple calculation, each triplet is about 40 meters long with regular quadrupoles. The length of one bending angle compensation section can be reduced from 250 meters to 130 meters. Therefore, the increase of the lattice circumference can be reduced to about 1.8 kilometers.

Based on the assumption that both electrons and positrons can be generated by polarized particle source, we design spin rotators for e^+ and e^- rings for CEPC. However, it is also beneficial for physics programs if longitudinal polarization is only achieved for electrons, if matured polarized e^+ source is still not available. In this case, spin rotators are not needed in the e^+ ring. Fig. 12 shows the geometry of the e^+/e^- rings with spin rotators only in the e^- ring. Upstream of the IR of the e^- ring, the bending angle compensation section $\Delta\theta_1$ and $\Delta\theta_2$ are needed following the spin rotator (rotatorU). Downstream of the IR, only the bending angle compensation section $\Delta\theta_1$ is needed prior to the spin rotator (rotatorD). Considering the length reduction potential of the bending angle compensation sections, the increase of the circumference can be further reduced to 1.18 km.

In addition, the bending angle compensation section $\Delta\theta_1$ can be incorporated into the IR, in case of a redesign of the CEPC lattice. Thereby, the increase of the circumference can be further reduced to 660 m for longitudinal polarized e^- beam alone or 1.28 km for longitudinal polarized e^-/e^+ beams.

If the crossing angle at the IP can be changed on the assumption that the CEPC collider ring lattice will be redesigned for running with longitudinal polarization in the future. The following formulas need to be satisfied

$$\begin{aligned} a\gamma(\theta_u + \Delta\theta) &= -\frac{\pi}{2} \\ a\gamma(C_d(\theta_d + \theta_{dd}) + \Delta\theta) &= \frac{\pi}{2} \\ \theta''_{\text{IR}} = -\theta'_c + C_d(\theta_d + \theta_{dd}) + \Delta\theta &= \theta'_c + \theta_u + \Delta\theta \end{aligned} \quad (17)$$

All the bending angles of the dipoles in the downstream of the IR need to be multiplied by C_d , which equals to 0.808. And the crossing angle is $2\theta'_c =$

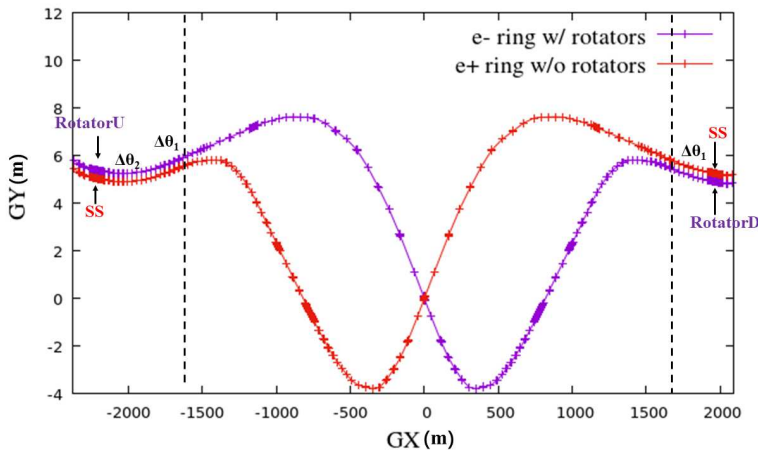


Fig. 12 Geometry of the e^+/e^- rings with spin rotators only for e^- beams.

30.35 mrad. Here the bending angle compensation section $\Delta\theta = 4.04$ mrad, which can be incorporated into the IR. In this case, the increase of the collider ring length is only contributed by the four spin rotators. Hence, the increase can be reduced to about 400 m for longitudinal polarized e^- beam alone or for longitudinal polarized e^-/e^+ beams.

6 Summary

As a key research topic in implementing longitudinal polarized beams for CEPC at Z-pole, the designs of solenoid-based spin rotators for the CEPC collider rings are discussed in this article. And different insertion schemes of the spin rotators are compared. Then, we presented an optimized insertion schemes with a complete spin rotator design. Simulation results shows that high longitudinal beam polarization can be achieved at the IP and the influence to the orbital motion is acceptable.

At this stage our models do not have misalignments for the whole collider ring. However, the simulation of realistic misalignments and the modeling of the correction of the orbital imperfections are very important for beam polarization at ultra-high beam energies. These topics will be studied in the future on the basis of this simulation framework, and will be an integral part of investigation of feasibility of attaining high beam polarization at CEPC.

There is still room for further optimization of the dynamic apertures and the length of spin rotators. As we discussed in Chapter 5, the length growth of the collider ring can be reduced to 1.8 km for e^+/e^- longitudinal polarization and to 1.18 km for e^- longitudinal polarization based on the current CEPC CDR lattice design. In case of a redesign of CEPC lattice, if the crossing angle can be modified to 30.35 mrad and the IR region are adjusted accordingly, the total length occupied by the insertion of the spin rotator can be reduced

to about 400 m for longitudinal polarized e^- beam alone or for longitudinal polarized e^-/e^+ beams.

Acknowledgments. The authors are especially grateful to Dr. Sergei Nikitin for the helpful discussion and the proofreading. This study was supported by National Natural Science Foundation of China (Grant No. 11975252); National Key Program for S&T Research and Development (Grant No. 2016YFA0400400 and 2018YFA0404300); Key Research Program of Frontier Sciences, CAS (Grant No. QYZDJ-SSW-SLH004); Youth Innovation Promotion Association CAS (No. 2021012).

Declarations

On behalf of all authors, the corresponding author states that there is no conflict of interest.

References

- [1] CEPC Accelerator Study Group: Snowmass2021 White Paper AF3-CEPC. <https://arxiv.org/abs/2203.09451>
- [2] The CEPC Study Group: CEPC Conceptual Design Report: Volume 1 - Accelerator. <https://arxiv.org/abs/1809.00285>
- [3] D.T. Pierce, F. Meier, P. Zürcher: Direct observation of spin dependent electronic structure of GaAs using spin polarized photo emission. Physics Letters A **51**(8), 465–466 (1975)
- [4] Z. Duan, J. Gao, X. P. Li et al.: Concepts of longitudinally polarized electron and positron colliding beams in the Circular electron positron collider. in *Proc. of IPAC2019*, Melbourne, Australia, paper MOPMP012 (2019)
- [5] Positron Working Group Collaboration: Report on the ILC Postron Source (2018). PUBDB-2019-00651
- [6] E. Voutier for the PEPPo Collaboration: Polarized positron production at MeV electron accelerators (2017). <https://doi.org/10.48550/arXiv.1711.09659>
- [7] The LEP Collaborations: ALEPH Collaboration, DELPHI Collaboration, L3 Collaboration, OPAL Collaboration, the LEP Electroweak Working Group, the SLD Heavy Flavour, Electroweak Working Group: A Combination of Preliminary Electroweak Measurements and Constraints on the Standard Model. arXiv:hep-ex/0312023 (2004)

- [8] D.P. Barber, M. Böge, H.D. Bremer et al.: The first achievement of longitudinal spin polarization in a high energy electron storage ring. *Physics Letters B* **343**(1), 436–443 (1995)
- [9] J. Buon, K. Steffen: HERA variable-energy “mini” spin rotator and head-on ep collision scheme with choice of electron helicity. *Nucl. Instrum. Methods A* **245**, 248 (1986)
- [10] V. I. Ptitsin, Y. M. Shatunov, S. Peggs: Helical spin rotators and snakes for RHIC (1995). <https://www.osti.gov/biblio/61200>
- [11] D. P. Barber, J. Kewisch, G. Ripken et al.: A solenoid spin rotator for large electron storage rings. *Particle Accelerators* **17**, 243–262 (1985)
- [12] I.A. Koop: Longtidinally polarized electron in SuperB. In: The 40th ICFA Advanced Beam Dynamics Workshop on High Luminosity $e^+ e^-$ Factories (2008)
- [13] M.E. Biagini, P. Raimondi, P. Piminov et al.: Super-B lattice studies. in *Proc. of IPAC2010*, Kyoto, Japan, paper TUPEB004 (2010)
- [14] S. A. Nikitin: Opportunities to obtain polarization at CEPC. *International Journal of Modern Physics A* **34**(13&14) (2019)
- [15] S. A. Nikitin: Polarization issues in circular electron–positron supercolliders. *International Journal of Modern Physics A* **35**(15&16) (2020)
- [16] J. Adam, W. Akers, A. Arno et al.: Electron Ion Collider Conceptual Design Report (2021). https://www.bnl.gov/ec/files/eic_cdr_final.pdf
- [17] V. Ptitsyn, C. Montag, S. Tepikian: Electron polarization in the eRHIC ring-ring design. in *Proc. of IPAC2016*, Busan, Korea, paper THRMR010 (2016)
- [18] P. Chevtsov, Y. Derbenev, G. Kraft et al.: Universal Synchronous Spin Rotators for Electron-Ion Colliders. <https://arxiv.org/pdf/1606.02419.pdf>
- [19] N. Wang, U. Wienands: Spin Rotator Design for SuperKEKB (2019). https://indico.fnal.gov/event/21420/sessions/5962/attachments/39120/47402/Spin-Rotator_Ningdong_Wang.pdf
- [20] SAD Home Page. <https://acc-physics.kek.jp/SAD/>
- [21] D. Sagan: The Bmad Reference Manual. <https://www.classe.cornell.edu/bmad/manual.html>
- [22] E. Forest, F. Schmidt, E. McIntosh: Introduction to the polymorphic

24 *Investigation of spin rotators in CEPC at Z-pole*

- tracking code. CERN-SL-2002-044-AP, KEK report 2002-3 (2002)
- [23] D.M. Zhou, H. Koiso, A. Morita et al.: Lattice translation between accelerator simulation codes for SuperKEKB. in *Proc. of IPAC2016*, Busan, Korea, paper WEPOY040 (2016)
- [24] L.H. Thomas: The kinematics of an electron with an axis. *Phil. Mag.* **3**(1) (1927)
- [25] V. Bargmann, L. Michel, V.L. Telegdi: Precession of the polarization of particles moving in a homogeneous electromagnetic field. *Phys. Rev. Lett.* **2**(435) (1959)
- [26] D. P. Barber, G. Ripken: Computing Algorithms for e^+/e^- Polarization in Storage Rings. In: *Handbook of Accelerator Physics and Engineering* vol. 2, 3rd edn., pp. 194–195. World Scientific, Singapore (2013)
- [27] S.R. Mane: Synchrotron sideband spin resonances in high-energy electron storage rings. *Nuclear Instruments and Methods in Physics Research A* **292**(1), 52–74 (1990)
- [28] A. A. Sokolov, I. M. Ternov: On polarization and spin effects in the theory of synchrotron radiation. *Sov. Phys. Dokl.* **8**, 1203 (1964)
- [29] V. N. Baier, V. M. Katkov: Processes in high energy particle motion in magnetic field (1967). PRINT-67-2019
- [30] Y.S. Derbenev, A.M. Kondratenko: Polarization kinematics of particles in storage rings. *Sov. Phys. JETP* **37**, 968 (1973)
- [31] SuperB Collaboration: SuperB: A High-Luminosity Asymmetric e^+e^- Super Flavor Factory. Conceptual Design Report. <https://doi.org/10.48550/arXiv.0709.0451>
- [32] V.N Litvinenko, A. A. Zholtens: Compensating effect of solenoids with quadrupole lenses (1981). Novosibirsk Preprint 81-80, English translation: DESY Internal report DESY L-Trans 289
- [33] W.H Xia, J. Gao, Y.W. Wang et al.: CEPC Z-pole polarization design studies. *International Journal of Modern Physics A*, 2142003 (2021)
- [34] Y.W. Wang, F. Su, S. Bai et al.: Lattice design for the cepc double ring scheme. *International Journal of Modern Physics A* **33**(2) (2018)
- [35] Z. Duan, M. Bai, D.P. Barber et al.: A monte-carlo simulation of the equilibrium beam polarization in ultra-high energy electron (positron) storage rings. *Nuclear Instruments and Methods in Physics Research A* **793**, 81–91 (2015)

- [36] B. Wang et al.: Imperfection and correction for CEPC. presented at the IAS program on high energy physics (HEP 2021), Hongkong (2021). (To be published)
- [37] W.H. Xia, Z. Duan, Y.W. Wang et al.: Evaluation of radiative depolarization in the future circular electron-positron collider. (To be published)
- [38] A. M. Kondratenko: Polarization stability of opposite-moving beams. *Zh. Eksp. Teor. Fiz.* **66**, 1211–1218 (1974)